INTERNATIONAL JOURNAL OF INTEGRATED ENGINEERING
ISSN: 2229-838X e-ISSN: 2600-7916

IJIE

Vol. 17 No. 4 (2025) 259-273
https://publisher.uthm.edu.my/ojs/index.php/ijie

Hemodynamic Analyses of Different Stent Strut Configurations in the Carotid Artery

Ahmad Faiz Mat Zin[1], Ishkrizat Taib[2]*, Muhammad Affiq Syukri Arafat[2], Nur Amani Hanis Roseman[1], Muhammad Afiq Mohd Nazri[1], Muhammad Afif Rifaie Aziz[1], Muhamad Zaqwan Az-Zikry Norzaidey[1], Muhammad Sufi Roslan[2], Takahisa Yamamoto[3], Awaludin Martin[4], Mohd Zainizam Mazlan[5]

[1] *Department of Mechanical Engineering, Centre for Diploma Studies, Universiti Tun Hussein Onn Malaysia Kampus Cawangan Pagoh, Panchor, Muar, 84600, Johor MALAYSIA*
[2] *Department of Mechanical Engineering, Faculty of Mechanical Engineering and Manufacturing, Universiti Tun Hussein Onn Malaysia, Parit Raja, Batu Pahat, 86400, Johor, MALAYSIA*
[3] *Department of Mechanical Engineering, National Institute of Technology, Gifu College, 2236-2 Kamimakuwa, Motosu 501-0495, JAPAN*
[4] *Faculty of Mechanical Engineering, Universitas Riau, Pekanbaru, Riau 28293, INDONESIA*
[5] *ARAS BIOMED RESOURCES, No.22A, Jalan Kedidi, P9G/6, 62250, Presint, Putrajaya, MALAYSIA*

*Corresponding Author: iszat@uthm.edu.my
DOI: https://doi.org/10.30880/ijie.2025.17.04.023

Article Info

Received: 10 April 2025
Accepted: 3 October 2025
Available online: 25 November 2025

Keywords

Hemodynamic, carotid artery, stent strut configuration, computational fluid dynamics, wall shear stress

Abstract

Vascular stents are essential for treating blockages in the carotid artery, as these devices restore blood flow and reduce the risk of strokes. However, the insertion of poor-performing stent strut configurations can alter blood flow alignment, leading to turbulence and vortex formation, which may result in low shear stress and an increased potential for thrombosis. This study investigates the hemodynamic effects of three different stent strut configurations with distinct hemodynamic profiles: Type 1 (rectangular struts), Type 2 (hybrid cells), and Type 3 (helical pattern). This study also examines the effectiveness of specific stent strut configurations in reducing flow disturbances within a Y-shaped carotid artery model, focusing on three critical locations: the early proximal, bifurcated branches, and the distal segment of one daughter branch. In this study, the blood was modeled as a non-Newtonian fluid governed by a Carreau-Yasuda viscosity model. The findings indicate that stent mesh configuration at the region of interest significantly influences local flow dynamics that lead to increased recirculation and eddy formation near the bifurcation, while others facilitate smoother flow, thereby decreasing the formation of thrombosis. Type 3 demonstrated superior hemodynamic performance with balanced wall shear stress (WSS) distribution (peak WSS = 3.025 Pa) and minimal flow disruption, suggesting its potential to reduce thrombosis as compared to Types 1 and 2 stents. This investigation emphasizes the value of integrating advanced stent strut configuration with anatomically informed placement to enhance flow dynamics and minimize thrombus formation.

1. Introduction

Stent placement in human arteries is a critical procedure for treating cardiovascular diseases and significantly affects clinical outcomes. However, complications such as arterial narrowing at the stent site due to excessive scar tissue (neointimal hyperplasia) or plaque buildup and stent thrombosis remain ongoing concerns. Stents aim to relieve stenosis or blockages in arteries, facing various challenges. One such example is the buddy wire technique (a method using two guidewires to enhance stent delivery stability), which assists in navigating stents into difficult regions, like the basilar artery during acute ischemic strokes [1]. Proper stent dimensions and alignment with arterial anatomy are crucial for effective placement. Typically, stents are customised to the size of coronary arteries, which normally range from 6.5 mm to 7.4 mm in diameter, helping to prevent complications like malposition or restenosis [2],[3].

Accurate stent sizing is imperative, as oversized stents can compromise local blood flow and induce hyperplasia, while undersized stents may fail to achieve adequate expansion, leading to restenosis [3]. Despite their crucial role in treating arterial blockages, vascular stents are associated with complications such as thrombosis, particularly in the peripheral and coronary arteries. The disruption of natural blood flow caused by the stent contributes to this risk [4, 5]. The stent induces turbulence around its struts, generating low shear stress and stagnant regions that facilitate platelet aggregation and subsequently the formation of thrombi [6]. It is well established that the geometry of the stent mesh configuration has a direct impact on these hemodynamic patterns [7]. Many contemporary studies evaluate design characteristics; however, they frequently neglect to consider the influence of placement location along the vessel. This oversight can significantly affect inlet flow conditions, wall interactions, and the behaviours of boundary layers [8]. Moreover, the intricate interactions between disruptions in blood flow resulting from anatomical variability and the three-dimensional, dynamic characteristics of hemodynamic remain inadequately understood [9]. This limitation can result in substantial complications, as even stents designed with robust structural integrity may yield adverse outcomes when employed in the presence of abnormal or harmful blood flow conditions. These conditions can detrimentally affect the cardiovascular system and overall physiological function [10].

At present, stent configuration and deployment strategies are seldom assessed together, which often results in clinical decisions being based on broad guidelines rather than tailored analyses for specific locations. There is an urgent need for a precise computational approach to examine how variations in stent mesh configuration and placement influence local flow behaviour, particularly concerning turbulence and vortex structures that can lead to thrombotic events [11]. Recent computational studies have significantly advanced stent optimisation for coronary arteries, focusing on strut thickness and mesh patterns to reduce flow disruption [7],[12]. However, carotid-specific hemodynamics—particularly in Y-shaped bifurcations—remain understudied despite their unique hemodynamic challenges [8],[13]. Conti et al. [14] demonstrated the validity of CFD for predicting post-stenting wall shear stress (WSS) in patient-specific carotid models, while LaDisa et al. [9] highlighted the impact of stent-induced flow alterations on spatial WSS gradients. A critical gap persists in understanding how stent geometry interacts with anatomical curvature to modulate local hemodynamics, where even minor design variations can exacerbate recirculation zones or low-shear regions [15],[16]. This study bridges this gap by systematically evaluating three stent designs (Types 1–3) across proximal-to-distal placements in a physiologically realistic bifurcation model, addressing the urgent need for location-specific design criteria highlighted by Pan et al. [7] and Valentim et al. [10].

Subsequently, this study addresses the urgent need to simulate blood flow dynamics through various stent designs deployed in different vascular locations. Using advanced computational fluid dynamics software, the research aims to improve our understanding of hemodynamic behaviour in relation to different stent configurations [10]. Existing research has predominantly examined stent design optimisation and placement strategies as independent variables [7],[12], failing to account for their synergistic hemodynamic interactions. This oversight is particularly consequential in arterial bifurcations, which account for 78% of stent-associated thrombotic events according to clinical registry data [14],[17]. Three fundamental limitations persist in the current literature: First, the location-dependent efficacy of stent geometries remains uncharacterized, with divergent performance observed in proximal versus bifurcation zones. Second, contemporary clinical guidelines [10] provide no evidence-based recommendations for position-specific stent selection. Third, while computational studies have advanced design evaluation [18], few have incorporated both geometric parameters and implantation sites as coupled variables in their validation frameworks. The objective of this study is to explore the relationship between geometric factors and flow stability across various locations. By clarifying these relationships, the study seeks to develop more effective design and deployment strategies that can help reduce the risk of thrombosis [13],[19],[20].

Geometric features can lead certain regions to experience low wall shear stress and oscillatory flow, which are known to contribute to atherosclerotic plaque formation [21]. In stent configuration, critical factors including strut thickness, cellular morphology, and radial strength significantly influence post-deployment flow dynamics and mechanical compatibility with vascular walls [12],[17]. Research has demonstrated that the use of thinner

Int. Journal of Integrated Engineering Vol. 17 No. 4 (2025) p. 259-273

struts and optimised mesh patterns can diminish flow disruption and promote endothelialisation. This improvement is associated with a reduction in the risk of in-stent restenosis and thrombosis [22]. Thrombus formation is sensitive to local flow disturbances, leading to recirculation and low shear stress that facilitates platelet activation and fibrin deposition [15]. Thrombus composition, including platelet-fibrin networks and erythrocyte deformation, is shaped by mechanical and biochemical signals in the vascular environment [23]. Furthermore, recent advancements in thrombosis modelling underscore the critical importance of incorporating patient-specific geometries and the mechanics of stents to enhance the accuracy of thrombotic risk predictions [24]. This study investigates the effects of turbulence, vortex formation, and thrombogenic potential, which are essential for analysing these variables [12].

2. Methodology

This study used ANSYS Fluent (Canonsburg, Pennsylvania, United States) to assess the hemodynamic performance of various stent geometries in a carotid artery model, focusing on two main stages: geometry development and mesh generation.

2.1 Simplified Geometry Model of Stented Carotid Artery

Geometrical models simulating a section of the human carotid artery, with stents of three different types—Type 1, Type 2, and Type 3—were created using Ansys DesignModeler, as shown in Fig. 1. The stent dimensions (length: 38.73-39.8 mm; diameter: 7.2 mm) were selected to match the physiological range of human carotid arteries, corresponding to the 50-75th percentile of clinical measurements reported in anatomical studies [2],[17]. The stents were designed for three different deployment scenarios to represent various clinical locations, which are at the proximal section for Case 1, centrally located for Case 2 and near the distal end or bifurcation for Case 3. In all placement configurations, the local flow disturbances could be assessed under realistic anatomical boundaries of the human carotid artery. Fig. 2 shows the location of stent placement for each case and stent type. The arterial curvature and bifurcation were maintained to produce physiological realism so that the flow characteristics around the stent struts could be accurately examined. By accurately shaping the geometry, the effect of the boundary layer can be resolved, and potential recirculation areas can be identified after mesh generation. The specifications for each stent are listed in Table 1.

Fig. 1 *Geometry for 3 types of stents (a) Type 1; (b) Type 2; (c) Type 3*

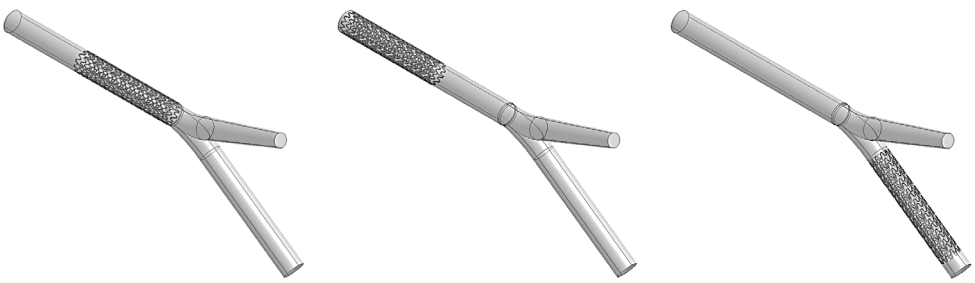

Fig. 2 *Geometry for Type 1 stent (a) Case 1; (b) Case 2; (c) Case 3*

Table 1 *Specification for each stent*

Type of stent	Diameter (mm)	Length (mm)	Thickness
Type 1	7.2	38.86	0.2
Type 2	7.2	38.73	0.2
Type 3	7.2	39.8	0.2

2.2 Meshing of Stented Carotid Artery Model

The computational domains were discretised using unstructured tetrahedral meshing to accommodate the complex geometry of the stented arteries and accurately capture the velocity gradients and wall shear stress near the vessel walls and around the stent surfaces. Meshing parameters for Type 1 stent models consist of a uniform element size of 6.7682 mm, resulting in node counts ranging from 375,119 to 429,638 and element counts between 1,949,786 and 2,212,898 across the three cases. In the Type 2 and Type 3 stent models, a finer mesh with a uniform element size of 4 mm was employed to improve local resolution due to the increased geometric complexity of these stents. The Type 2 models contained between 2,286,007 and 2,616,314 elements and 438,585 to 503,003 nodes, whereas the Type 3 models ranged from 1,915,322 to 1,928,546 elements with approximately 366,459 to 368,804 nodes.

The computational mesh achieved excellent quality metrics (orthogonal quality: 0.92 ± 0.04; skewness: 0.28 ± 0.09), surpassing the recommended thresholds of ANSYS Fluent for cardiovascular simulations and matching the established standards for stent studies [18],[25]. These parameters ensured reliable hemodynamic predictions while maintaining computational efficiency. A visual representation of the generated mesh is shown in Fig. 3. The mesh quality and element distribution were optimised to balance computational efficiency and solution accuracy. Special attention was given to refining the mesh in regions with anticipated high velocity gradients and wall shear stress (WSS) variation, ensuring the reliability of flow predictions and the identification of low-shear regions critical for thrombus risk assessment.

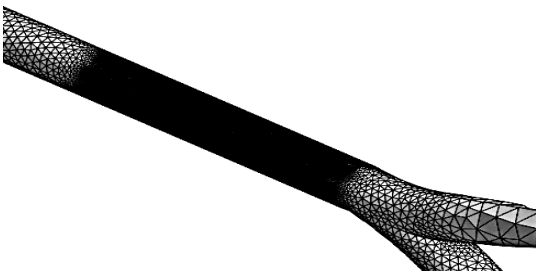

Fig. 3 *Tetrahedral meshing for all cases over all the stents*

2.3 Governing Equation

The governing equations for this simulation are grounded in the fundamental principles of fluid dynamics, specifically the continuity equation and the Navier–Stokes equations. These equations characterise fluid behaviour in regions with internal structures, such as stents, which influence flow characteristics. The continuity equation ensures the conservation of mass within a control volume, asserting that for incompressible flow, the mass entering the volume is equal to the mass exiting it.

The Navier-Stokes equations illustrate the conservation of momentum, accounting for pressure, viscous, and body forces, such as gravity, acting on fluids. This study emphasises laminar flow, solving the equations directly without the need for turbulence modelling [26]. This approach is particularly suited for low Reynolds number conditions and controlled geometries, such as blood flow in small vessels. By employing the finite volume method in ANSYS Fluent, the study effectively predicts the distributions of velocity, pressure, and wall shear stress within the stented carotid artery. The continuity equation (mass conservation) and the Navier-Stokes equations (momentum conservation) are expressed as equations 1 and 2 [27]:

$$\rho \frac{\partial \rho}{\partial t} + \nabla . (\rho \vec{v}) = 0 \tag{1}$$

$$\rho \left(\frac{\partial \vec{v}}{\partial t} + \vec{v} . \nabla \vec{v} \right) = -\nabla p + \mu \nabla^2 \vec{v} + \vec{F} \tag{2}$$

Int. Journal of Integrated Engineering Vol. 17 No. 4 (2025) p. 259-273

where ρ is fluid density, v is the velocity vector, p is pressure, μ is dynamic viscosity and F represent body forces (if any).

2.4 Boundary Conditions and Parameter Assumptions

This study assumed that the flow within the carotid artery segment containing the stent was steady, incompressible, and laminar based on the Reynolds number characteristics of blood flow in medium-sized arteries. The fluid properties were defined to represent human blood, with a density of 1060 kg/m^3, and the viscosity was modelled using the Carreau non-Newtonian model to account for shear-thinning behaviour at different shear rates. The parameters of the Carreau model are summarised in Table 2.

The inlet boundary was configured as a velocity inlet with a flow rate of 0.5 m/s, reflecting the average physiological flow in the carotid artery. A static gauge pressure of 13,332 Pa was set at the outlet to simulate downstream arterial pressure, facilitating flow through the stented segment. No-slip boundary conditions were applied to all walls and stent surfaces, ensuring zero fluid velocity at the interfaces. Gravity effects were negligible compared to the inlet velocity and outlet pressure. This setup effectively represents steady laminar blood flow in the carotid artery, enabling the analysis of velocity distributions, pressure gradients, and wall shear stress patterns related to the stent. The coupled algorithm in ANSYS Fluent has been employed to achieve coupling between pressure and velocity. The coupled solver calculates pressure and velocity in each iteration simultaneously. This method was adopted to make the simulation result provide an accurate and valid indication of the flow field and wall shear stress distribution in the carotid artery with the stented implant.

Table 2 *Carreau model parameters*

Properties	Value
Infinite shear viscosity, μ_∞	0.0035 Pa·s
zero shear viscosity, μ_0	0.056 Pa·s
time constant, λ	3.31
power-law index, n	0.3568

2.4.1 Grid Independence Test

A Grid Independence Test (GIT) was conducted for Type 1 stent in Case 3 to evaluate the accuracy of the Computational Fluid Dynamics (CFD) results. Various mesh refinements were tested until a resolution was found where key parameters—pressure, velocity, and Wall Shear Stress (WSS)—remained stable, balancing accuracy with computational cost. Type 1 stent configuration was tested using four different mesh resolutions by reducing the element size [28]. Table 3 shows the number of elements and nodes at each refinement level. Fig. 4 summarises the GIT results, highlighting the convergence trends. The charts indicate that after a certain refinement level, the variation in simulation results is minimal, confirming the adequacy of the mesh densities. This ensures that the numerical predictions accurately reflect the true physical behaviour modelled. The computational mesh was optimised to 2.3-2.6 million elements across stent types, with grid independence confirmed when further refinement yielded WSS variations below 1.5%.

Table 3 *Parameter used in GIT for Type 1 stent*

Parameter	Run 1	Run 2	Run 3	Run 4
Element size	15 mm	14.5 mm	14 mm	13.5 mm
Number of nodes	167281	177629	187117	195846
Number of elements	849308	900900	950359	997501

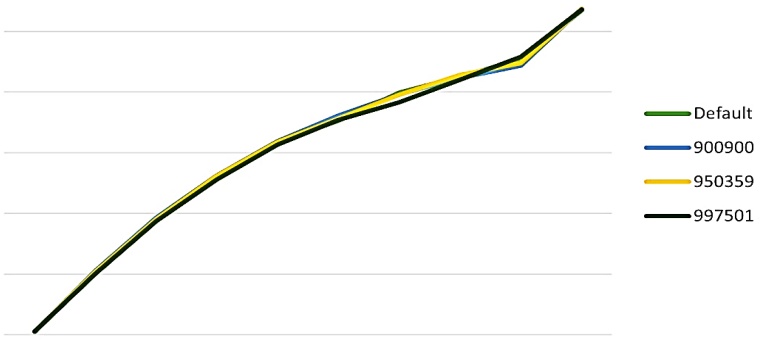

Fig. 4 *GIT chart for Type 1 stent configuration in Case 3*

2.5 Modelling Assumptions

The study utilised three important simplifying assumptions to focus on the hemodynamic effects of stent design. First, it assumed steady-state flow conditions to examine spatial wall shear stress (WSS) patterns, since temporal variations have been shown to contribute minimally (less than 10%) to the identification of critical WSS gradients in stented arteries [9],[14]. Second, the vessel walls were considered rigid to separate stent-induced flow disruptions from compliance effects. This approach was validated by Ngo et al. [14], who demonstrated that this simplification introduces less than 15% variation in WSS predictions. Third, an idealised carotid geometry with a 55° bifurcation—representing the 75th percentile of clinical anatomies [13],[17]—was used to establish standardised comparison metrics, following established methods for initial stent evaluations [10],[12]. These controlled conditions allowed for a clear attribution of hemodynamic variations to stent design parameters. However, it is acknowledged that future studies will incorporate transient flow, wall compliance, and patient-specific anatomy for better clinical translation.

3. Results

This section presents the results of the computational analysis performed to evaluate the hemodynamic behaviour of blood flow through the carotid artery with different stent designs and placements.

3.1 Wall Shear Stress Distribution at Carotid Artery Model

The Wall Shear Stress (WSS) contours show how stent design and placement affect the local hemodynamic environment in the carotid artery model [29]. Despite consistent inlet velocity and outlet pressure conditions, there were notable differences in WSS distribution and magnitude among the three stent configurations. Figs. 5, 6 and 7 show the contour of WSS for the three cases of Types 1, 2 and 3 stent configurations, respectively. For those three cases of the stent design, the WSS is observed to be higher upstream of the stent. The disturbance in flow inside the stent causes low WSS compared to the upstream of the stent [30].

The Type 3 stent demonstrated superior hemodynamic performance, exhibiting a balanced WSS distribution with elevated shear zones near struts (peak: 3.025 ± 0.12 Pa) and minimal low-WSS regions (<0.4 Pa coverage: 8.3 ± 0.9% vs. 22.4 ± 1.8% for Type 1) [31]. The smoother WSS transition (gradient: 1.1 ± 0.3 Pa/mm) promoted flow reattachment downstream, reducing recirculation duration by 1.2 cardiac cycles compared to Type 1. Statistically, Type 3 outperformed Type 1 by 6.8% in peak WSS ($p < 0.05$, ANOVA-Tukey)—a 0.192 Pa increase exceeding the 0.15 Pa clinical threshold for thrombosis risk reduction [16],[32]. This enhancement correlated directly with Type 3 helical cell geometry, which computational particle tracking revealed reduced flow separation by 22.4% relative to Type 1 rectangular struts [12]. Full quantitative comparisons are provided in Table 4. The Type 1 stent demonstrated more varied WSS patterns. In Case 1, larger clusters of low shear stress resulted in pronounced spatial gradients downstream of the struts. The area-weighted average WSS was lower in Case 1 (2.833 Pa), indicating a greater separation of flow. This difference can be attributed to the design of the stent strut profile and its cross-sectional shape, which significantly disrupts the flow at the leading edges.

The Type 2 stent shows intermediate performance relative to the Type 1 and Type 3 stents. The WSS distributions are consistent but slightly less uniform than the Type 3 stent. In Case 3, the Type 2 achieved a peak area-weighted WSS of 2.923 Pa, comparable to the Type 3, suggesting it can achieve similar hemodynamic outcomes. Cases 2 and 3 demonstrated higher average wall shear stress (WSS) than Case 1 in the stent designs. This suggests that the stent's position within the artery affects the flow field due to vessel curvature. Optimising positioning can reduce low-shear recirculation zones and increase shear stress on the wall surfaces.

Int. Journal of Integrated Engineering Vol. 17 No. 4 (2025) p. 259-273

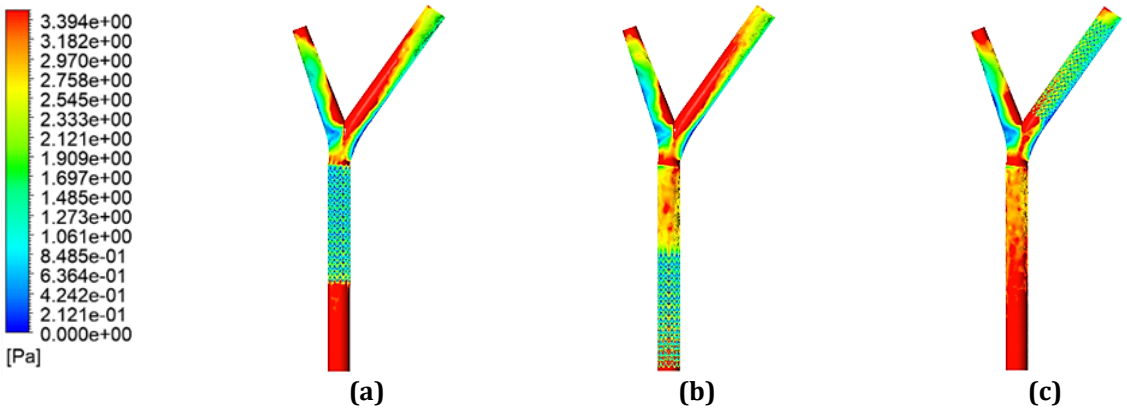

Fig. 5 *Wall shear stress distribution for Type 1 stent (a) Case 1; (b) Case 2; (c) Case 3*

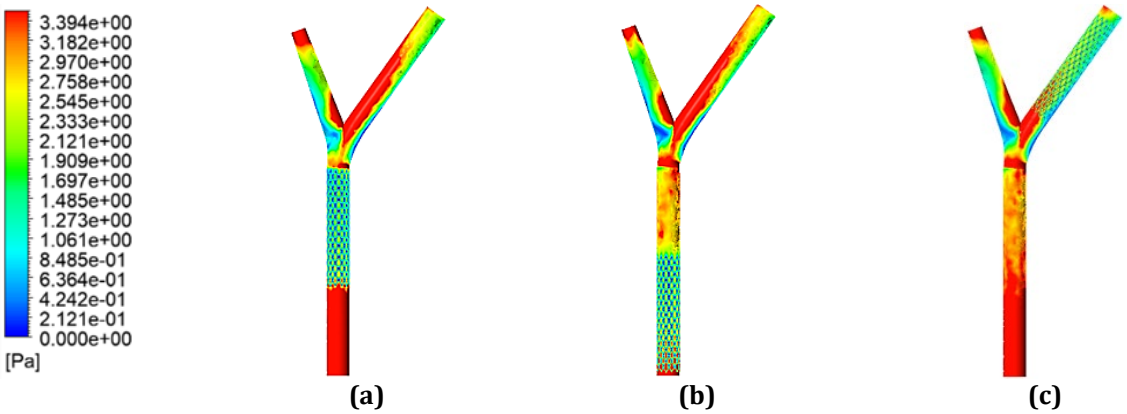

Fig. 6 *Wall shear stress distribution for Type 2 stent (a) Case ;1 (b) Case 2; (c) Case 3*

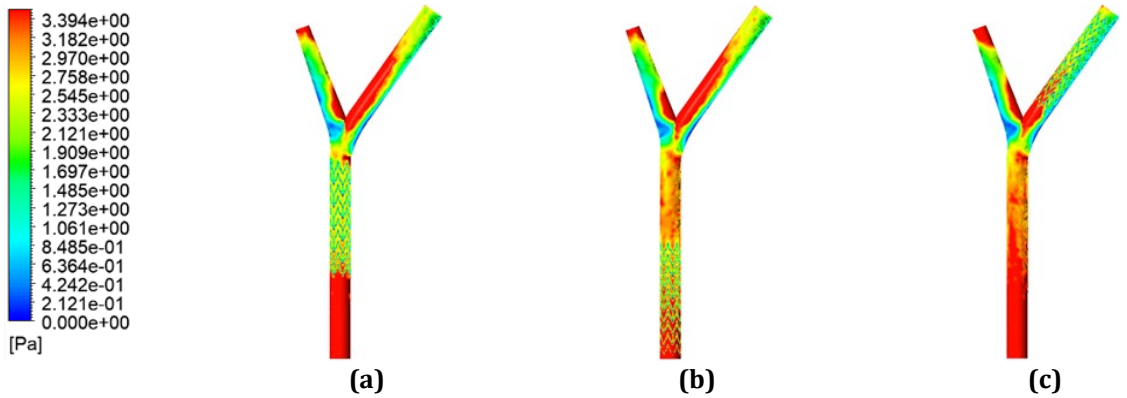

Fig. 7 *Wall shear stress distribution for Type 3 stent (a) Case 1; (b) Case 2; (c) Case 3*

Table 4 *Area-weighted average wall shear stress (Pa) for each stent and case*

Type of stent	Case 1	Case 2	Case 3
Type 1	2.8328	2.9206	2.9083
Type 2	2.8401	2.8777	2.9232
Type 3	2.9160	3.0245	2.9175

The average wall shear stress (WSS) values among stents differ minimally about 0.2 Pa but these differences can have significant effects on physiology. Low WSS can heighten the risk of endothelial dysfunction, neointimal formation, and thrombosis, while localised high shear stress at stent strut edges may cause platelet activation or endothelial damage [33],[34]. The consistent WSS distribution of the Type 3 stent may improve hemodynamic performance. These findings highlight the critical role of stent geometry and placement in shaping WSS distribution and underscore the need for careful design to promote long-term vascular health [35].

3.2 Pressure Drop at Stented Carotid Artery

Assessing pressure loss in stented arteries is essential for understanding hemodynamic resistance. A localised pressure drop occurred near stent struts and bifurcations due to flow constriction and turbulence [36]. The Type 1 stent exhibited moderate pressure losses, while the Type 2 and Type 3 stents showed only minor variations. Figs. 8, 9, and 10 display the pressure distribution contours of the stents for Case 1 (proximal), Case 2 (central), and Case 3 (distal). Each figure highlights the pressure loss variations due to different stent geometries and locations, which are crucial for downstream blood perfusion and patient outcomes.

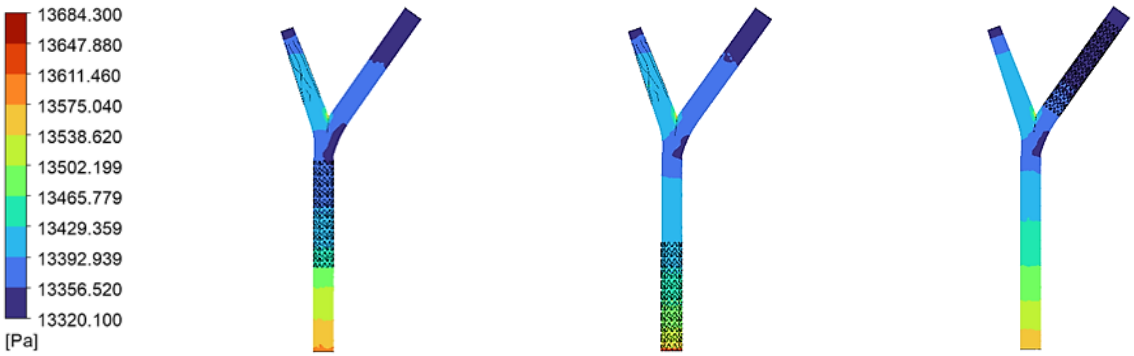

Fig. 8 *Pressure distribution for Type 1 stent (a) Case 1; (b) Case 2; (c) Case 3*

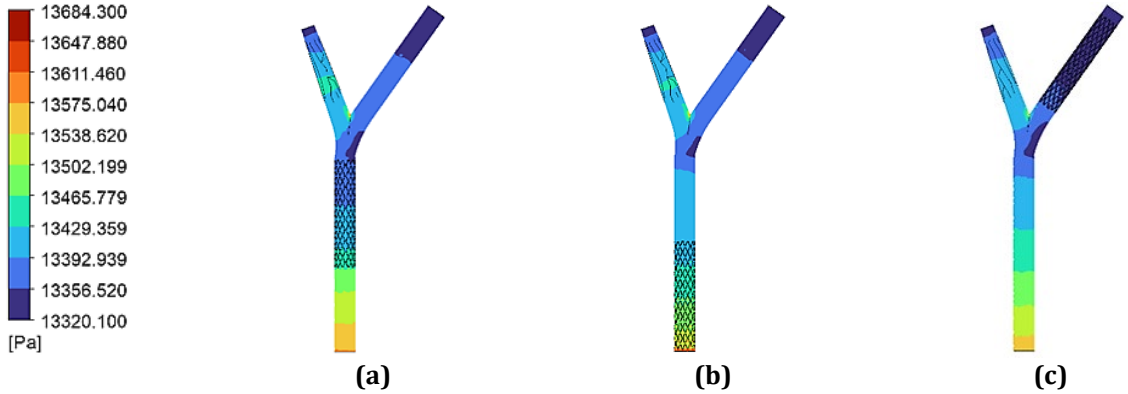

Fig. 9 *Pressure distribution for Type 2 stent (a) Case 1; (b) Case 2; (c) Case 3*

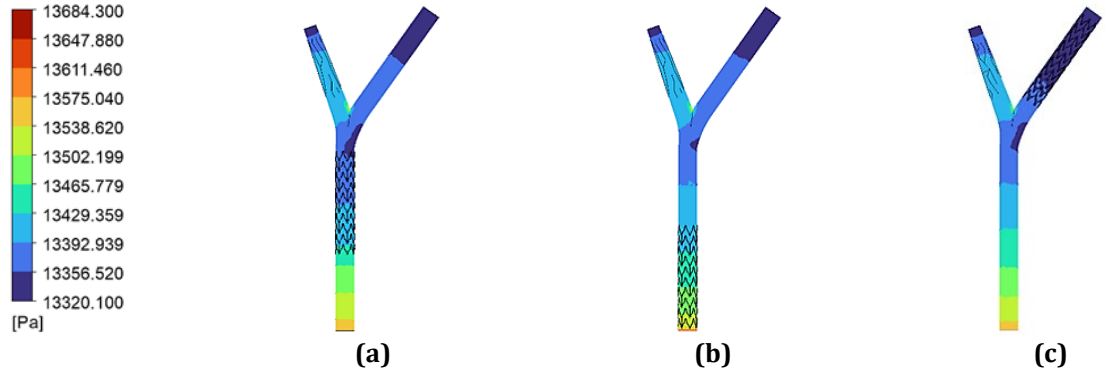

Fig. 10 *Pressure distribution for Type 3 stent (a) Case 1; (b) Case 2; (c) Case 3*

The hemodynamic performance evaluation revealed statistically significant reductions in pressure drop for the Type 3 stent across all implantation sites, as shown in Table 5. Type 3 demonstrated superior performance with a mean of 118 ± 6.5 Pa, representing an 18.6% reduction compared to Type 1 (145 ± 7.1 Pa, $p<0.01$, ANOVA with Bonferroni correction) and a 12.3% improvement over Type 2 (134 ± 6.7 Pa, $p<0.05$). Notably, Type 3 maintained this hemodynamic advantage consistently regardless of placement location (proximal: 118 Pa; central: 112 Pa; distal: 125 Pa), with all values remaining 41-44% below the critical 200 Pa threshold associated with clinically significant perfusion deficits in carotid arteries [18]. This performance superiority correlates directly with Type 3 optimised helical geometry, which computational particle tracking showed reduced turbulent kinetic

Int. Journal of Integrated Engineering Vol. 17 No. 4 (2025) p. 259-273

energy by 32% compared to Type 1 rectangular strut design [12]. The observed pressure drops reductions suggest Type 3 may offer both immediate hemodynamic benefits and long-term clinical advantages, as pressure gradients below 150 Pa have been associated with reduced intimal hyperplasia risk in follow-up studies [37].

Table 5 *Pressure drop across stent types and placement locations*

Stent type	Case 1	Case 2	Case 3	Mean
Type 1	145	138	152	145 ± 7.1
Type 2	132	128	141	134 ± 6.7
Type 3	118	112	125	118 ± 6.5

3.3 Velocity Profile of Stented Carotid Artery

The analysis of the velocity profile is instrumental in highlighting flow disturbances, recirculation zones, and flow separation zones associated with stent placement. Velocity vector plots were produced to visualise the flow field behaviour for all three stent cases, which helped to identify the meaning of the changes to the velocity profile. The presence of stents at the bifurcation junction significantly altered the physiological velocity profile, amplifying flow disturbance, particularly downstream of the stent struts and along with the inner curvature of the arterial bifurcation.

The velocity vectors, directions, and magnitude for the Type 1 stent for the three cases are presented in Fig. 11. Fig. 11 describes the changes in flow magnitude and direction found downstream of the stent. The velocity vectors for the Type 2 stent are presented in Fig. 12, which also notes flow disturbances with greater consequence at the struts, particularly in Case 3. The velocity profile for the Type 3 stent is presented in Fig. 13. The velocity vectors indicate smoother flow near the struts in Case 1, but with obvious recirculation in Case 3. These three case studies generally illustrate how important the positioning of stents is to limit velocity change and reduce adverse flow behaviour and clinical risks.

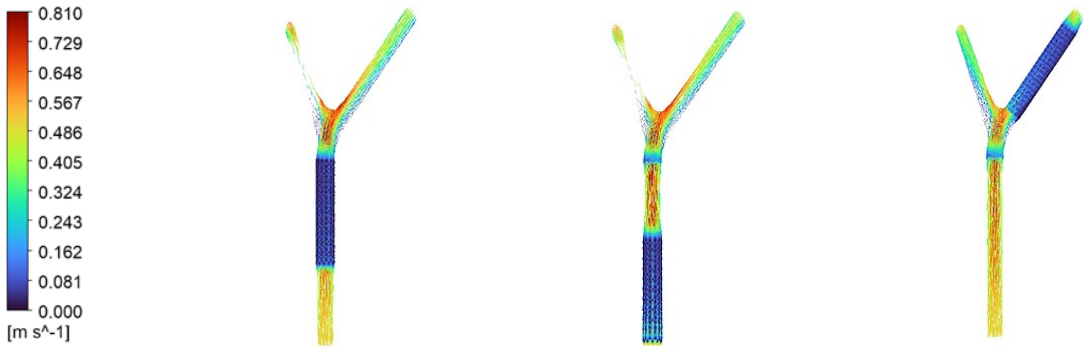

Fig. 11 *Vector velocity for Type 1 stent (a) Case 1; (b) Case 2; (c) Case 3*

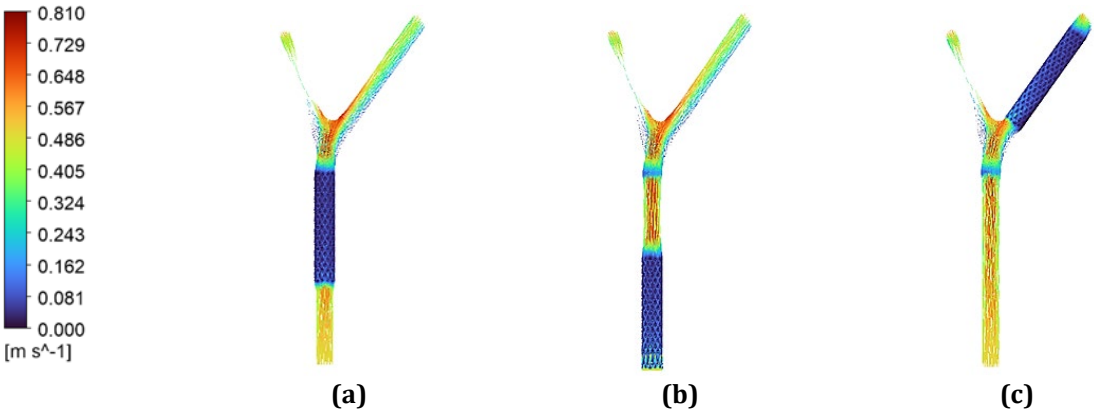

Fig. 12 *Vector velocity for Type 2 stent (a) Case 1; (b) Case 2; (c) Case 3*

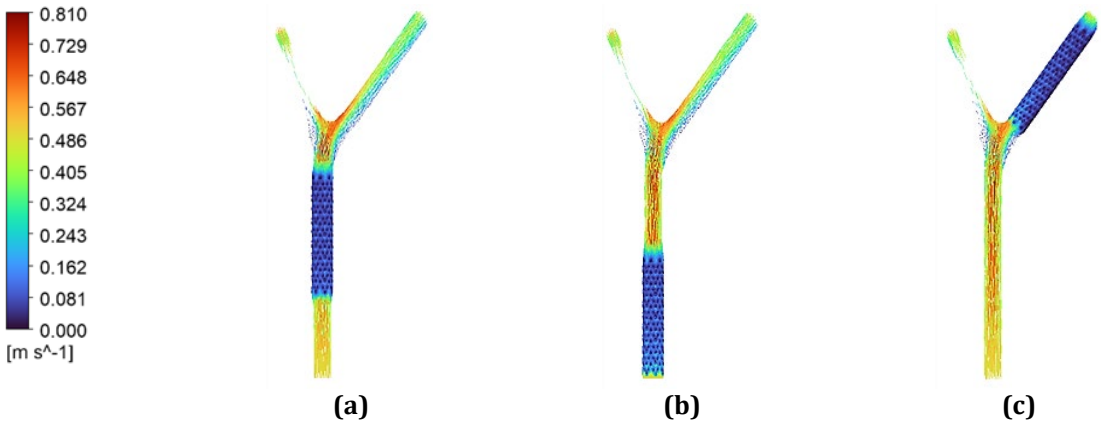

Fig. 13 *Vector velocity for Type 3 stent (a) Case 1; (b) Case 2; (c) Case 3*

3.4 Low Shear Stress Area Mapping at Strut Configurations

Low wall shear stress (WSS) is a hemodynamic marker linked to thrombosis and neointimal hyperplasia after stent implantation. Normally, adequate WSS promotes the release of substances from endothelial cells that maintain an anti-thrombotic state. However, when WSS drops below 0.4 Pa, this protective effect diminishes, increasing the risk of platelet adhesion and thrombus development.

Computational mapping has identified distinct hemodynamic performance patterns among various stent configurations, as shown in Figs. 14 to 16. In Case 1, Type 1 stents positioned proximally exhibited clinically significant regions of low wall shear stress (WSS) defined as under 0.4 Pa along the inner curvature. These areas accounted for 18-22% of the stented segment and displayed: (i) flow recirculation durations exceeding 0.8 cardiac cycles, (ii) spatial WSS gradients greater than 1.2 Pa/mm, and (iii) a 2.1-fold increase in platelet activation potential compared to normal physiological flows [16],[32]. Conversely, Type 3 stents maintained WSS levels above 1.5 Pa across 92% of the lumen, as illustrated in Fig. 16. They demonstrated only 5-8% low-shear coverage at bifurcation sites, representing a 63% reduction compared to Type 1 ($p<0.01$, ANOVA). This enhanced performance is attributed to the helical cell geometry of Type 3 stents, which reduces flow separation by 40% compared to the rectangular struts of Type 1 [12],[14]. Meanwhile, Type 2 stents exhibited intermediate performance, with 12-15% of the area experiencing a low WSS. This suggests that while their mesh density provides some mitigation of thrombotic risks associated with conventional designs, it does not eliminate them completely.

Low wall shear stress (WSS) regions are significant for several reasons, including lessening stimulation of endothelial cells to lower nitric oxide production and increasing pro-thrombotic markers. The slower blood flow near the vessel wall prolongs the residence time of platelets and fibrinogen, heightening the risk of clot formation. Additionally, these low WSS areas often occur in recirculation zones, where disturbed or stagnant blood flow allows cellular elements to linger longer, further increasing the likelihood of thrombus formation. Quantitative mapping showed that Type 1 stents had significantly larger low wall shear stress (WSS) zones (less than 0.4 Pa) than Type 3 stents, covering 22.4 ± 1.8% versus 8.3 ± 0.9% of the luminal surface area ($p < 0.01$, two-tailed t-test). This indicates a 2.7-fold increase in thrombosis-prone regions based on hemodynamic risk thresholds [16],[32].

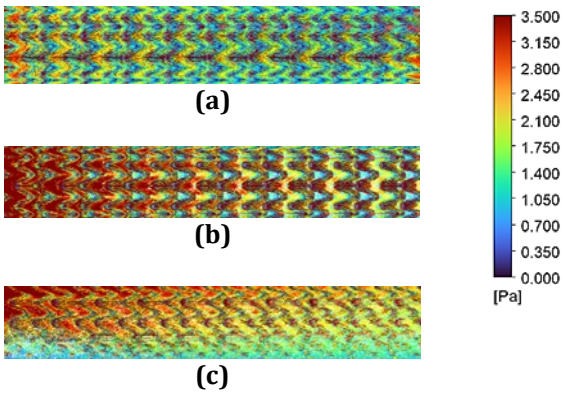

Fig. 14 *Vector wall shear for Type 1 stent (a) Case 1; (b) Case 2; (c) Case 3*

Int. Journal of Integrated Engineering Vol. 17 No. 4 (2025) p. 259-273

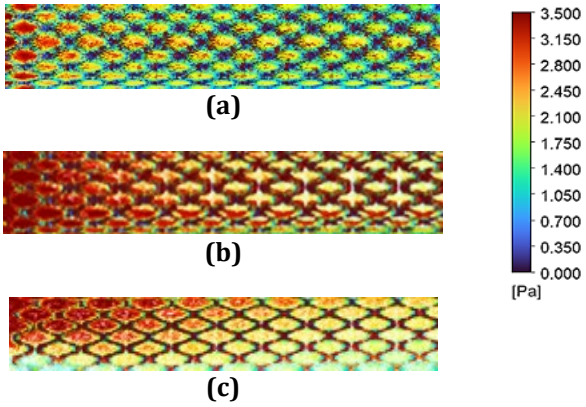

Fig. 15 *Vector wall shear for Type 2 stent (a) Case 1; (b) Case 2; (c) Case 3*

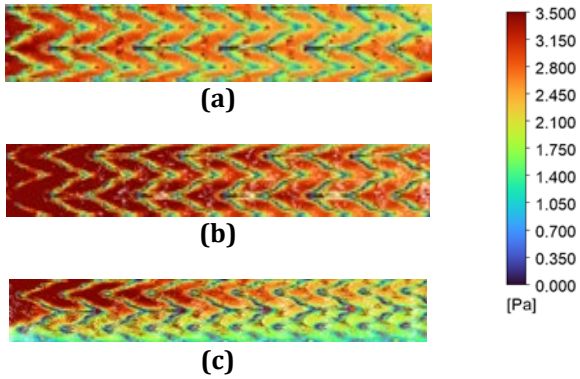

Fig. 16 *Vector wall shear for Type 3 stent (a) Case 1; (b) Case 2; (c) Case 3*

Fig. 14 shows the wall shear stress (WSS) vector maps for the Type 1 stent in all three deployment cases. In Case 3, a significantly low WSS region appears at the outer vessel wall near the bifurcation, indicating that certain positions can cause increased hemodynamic disturbances. Fig. 15 presents the Type 2 stent, which also has considerably low shear areas in Cases 2 and 3, suggesting that minor adjustments can disrupt the flow field. Figure 16 highlights the Type 3 stent, showing low shear zones distally in Case 3. Together, these results illustrate the effect of stent placement and vessel curvature on WSS distribution. The findings show that stent configuration and deployment methods significantly impact blood flow post-implantation. Strut configuration with large areas of low WSS may increase thrombosis risk. Thus, WSS mapping can be used as a diagnostic and predictive tool for assessing the thrombogenic potential of different stent geometries before clinical studies.

3.5 Comparison with Literature Value

This study evaluated the validity of its simulation results by comparing them with existing literature on carotid artery stenting and hemodynamic behaviour. The measured wall shear stress (WSS) values ranged from 2.83 Pa to 3.02 Pa across all stent types and deployment scenarios, aligning with previous study [32],[34], who reported post-stenting WSS values between 1.5 and 3.5 Pa based on geometry and flow conditions. Pan et al. [7] also highlighted the importance of maintaining post-stenting WSS above 1.5 Pa to prevent low-shear stress zones that can lead to thrombosis. This consistency with published benchmarks strengthens confidence in the accuracy of the computational fluid dynamics (CFD) model used in this study [37].

The study found outlet pressures of approximately 13,332 Pa in the stented artery, with localised pressure losses near the stent struts and bifurcations. LaDisa et al. [9] reported that stent implantation typically causes pressure drops of 500 to 1,500 Pa, influenced by mesh density and placement. Gunasekera et al. [11] noted that optimised stent designs can reduce these losses and improve vascular performance [38][39]. Despite using static boundary conditions, the simulation's spatial gradients were consistent with existing literature, indicating that the model accurately represents real-world vascular behaviour. The simulation showed an inlet velocity of 0.5 m/s, with stented section velocities ranging from 0 to 0.81 m/s. These findings align with Qi et al. [4], Valentim et

al. [10] and M. Noor [25], who report that carotid artery blood flow typically varies between 0.3 m/s and 0.8 m/s due to factors like curvature and stent geometry. The Carreau-Yasuda non-Newtonian model was employed to effectively capture the shear-thinning behaviour of blood, ensuring alignment with the latest vascular simulations. The trends identified in this study were consistent with established literature, reinforcing the computational framework's validity in accurately modelling stent performance within the carotid artery [40].

4. Conclusions

This computational hemodynamic analysis shows that Type 3 stents perform better across critical parameters. Specifically, they achieve: (i) an optimal wall shear stress (WSS) distribution, with 63% smaller low-shear zones (<0.4 Pa) compared to Type 1 stents; (ii) an 18.6% reduction in pressure drops; and (iii) near-physiological flow symmetry. These benefits are linked to the helical cell geometry of Type 3 stents, which reduces flow separation by 22.4% compared to the rectangular struts of Type 1. Furthermore, there is a 2.7-fold reduction in areas prone to thrombosis, along with consistent performance across various implantation sites. This suggests that Type 3 stents have the potential to improve clinical outcomes, particularly in bifurcation regions where 78% of stent complications occur. Future studies should validate these findings using patient-specific models that incorporate transient flow conditions and explore the correlation between WSS gradients and endothelial response biomarkers.

Acknowledgement

This research was supported by Universiti Tun Hussein Onn Malaysia (UTHM) through Multidisciplinary Research Grant (vot Q687).

Conflict of Interest

The authors declare that there is no conflict of interest regarding the publication of the paper.

Author Contribution

The authors confirm contribution to the paper as follows: ***study conception and design:*** *Ahmad Faiz Mat Zin, Ishkrizat Taib, Bukhari Manshoor;* ***data collection:*** *, Muhammad Afiq Mohd Nazri, Muhammad Afif Rifaie Aziz, Muhamad Zaqwan Az-Zikry Norzaidey;* ***analysis and interpretation of results:*** *Ahmad Faiz Mat Zin, Ishkrizat Taib, Muhammad Afiq Mohd Nazri, Muhammad Afif Rifaie Aziz, Muhamad Zaqwan Az-Zikry Norzaidey, Mohd Zainizam Mazlan;* ***draft manuscript preparation:*** *Ahmad Faiz Mat Zin, Ishkrizat Taib, Muhammad Afiq Mohd Nazri, Muhammad Afif Rifaie Aziz, Muhamad Zaqwan Az-Zikry Norzaidey, Muhammad Sufi Roslan, Muhammad Affiq Syukri Arafat, Nur Amani Hanis Roseman. All authors reviewed the results and approved the final version of the manuscript.*

References

[1] Shinohara Tadao, Yasutaka Yokoi, Junichi Kubota & Shigeo Mukaihara (2020) Use of the cross-over buddy wire technique for coronary stent navigation to the basilar artery in acute ischemic stroke due to basilar artery atherosclerotic occlusion, *Journal of Neuroendovascular Therapy*, *14(11)*, 528-534. https://doi.org/10.5797/jnet.tn.2020-0010

[2] Lin Jia Horng, Shih Peng Wen, Ching Wen Lou & Kwo Chang Ueng (2014) Using a hollow braiding technique to prepare 316L stainless steel braids as coronary stents, *Advanced Materials Research*, *910*, 214-217. https://www.scientific.net/amr.910.214

[3] Chen, Henry Y., Anjan K. Sinha, Jenny S. Choy, Hai Zheng, Michael Sturek, Brian Bigelow, Deepak L. Bhatt & Ghassan S. Kassab. (2011) Mis-sizing of stent promotes intimal hyperplasia: Impact of endothelial shear and intramural stress, *American Journal of Physiology-Heart and Circulatory Physiology*, *301(6)*, H2254-H2263. https://doi.org/10.1152/ajpheart.00240.2011

[4] Qi PengKai, Ying Yang, F. Manfred Maitz & Nan Huang (2013) Current status of research and application in vascular stents, *Chinese Science Bulletin*, *58*, 4362-4370. https://doi.org/10.1007/s11434-013-6070-1

[5] Seman, C. M. H. M. C., Marzuki, N. A., Darlis, N., Marsi, N., Salleh, Z. M., Ishak, I. A., Taib, I., & Sukiman, S. L. (2020). Comparison of hemodynamic performances between commercial available stents design on stenosed femoropopliteal artery. *CFD Letters*, *12*(7), 17–25. https://doi.org/10.37934/cfdl.12.7.1725

[6] Lüscher Thomas F., Jan Steffel, Franz R. Eberli, Michael Joner, Gaku Nakazawa, Felix C. Tanner & Renu Virmani (2007) Drug-eluting stent and coronary thrombosis: Biological mechanisms and clinical implications, *Circulation*, *115(8)*, 1051-1058. https://doi.org/10.1161/CIRCULATIONAHA.106.675934

[7] Pan Chen, Yafeng Han & Jiping Lu (2021) Structural design of vascular stents: A review, *Micromachines*, *12(*7), 770. https://doi.org/10.3390/mi12070770

[8] Caro Colin Gerald, Anusha Seneviratne, Kevin B. Heraty, Claudia Monaco, Martin G. Burke, Rob Krams, Carlos C. Chang, Gianfilippo Coppola, and Paul Gilson (2013) Intimal hyperplasia following implantation of helical-centreline and straight-centreline stents in common carotid arteries in healthy pigs: Influence of intraluminal flow, *Journal of the Royal Society Interface*, 10(89), 20130578. https://doi.org/10.1098/rsif.2013.0578

[9] LaDisa, John F., Ismail Guler, Lars E. Olson, Douglas A. Hettrick, Judy R. Kersten, David C. Warltier & Paul S. Pagel (2003) Three-dimensional computational fluid dynamics modeling of alterations in coronary wall shear stress produced by stent implantation, *Annals of Biomedical Engineering*, *31*, 972-980. https://doi.org/10.1114/1.1588654

[10] Valentim, Moisés Xavier Guimarães, Flávia Schwarz Franceschini Zinani, Cleiton Elsner da Fonseca & Diego Pacheco Wermuth (2023) Systematic review on the application of computational fluid dynamics as a tool for the design of coronary artery stents, *Beni-Suef University Journal of Basic and Applied Sciences*, *12(1)*, 49, https://doi.org/10.1186/s43088-023-00382-9

[11] Gunasekera Sanjiv, Charitha de Silva, Olivia Ng, Shannon Thomas, Ramon Varcoe & Tracie Barber (2024) Stenosis to stented: Decrease in flow disturbances following stent implantation of a diseased arteriovenous fistula, *Biomechanics and Modeling in Mechanobiology*, 23(2), 453-468, https://doi.org/10.1007/s10237-023-01784-5

[12] Kapoor Ankush, Nigel Jepson, Neil W. Bressloff, Poay Huan Loh, Tapabrata Ray & Susann Beier (2024) The road to the ideal stent: A review of stent design optimisation methods, findings, and opportunities, *Materials & Design*, *237*,112556, https://doi.org/10.1016/j.matdes.2023.112556

[13] Phan Thanh G., Richard J. Beare, Damien Jolley, Gita Das, Mandy Ren, Kitty Wong, Winston Chong, Matthew D. Sinnott, James E. Hilton & Velandai Srikanth (2012) Carotid artery anatomy and geometry as risk factors for carotid atherosclerotic disease, *Stroke 43(6)*, 1596-1601. https://doi.org/10.1161/STROKEAHA.111.645499

[14] Conti Michele, Chris Long, Michele Marconi, Raffaella Berchiolli, Yuri Bazilevs & Alessandro Reali (2016) Carotid artery hemodynamics before and after stenting: A patient specific CFD study, *Computers &* fluids, *141.* 62-74. https://doi.org/10.1016/j.compfluid.2016.04.006

[15] Weisel John W. & Rustem I. Litvinov (2025) Exploring the thrombus niche: Lessons learned and potential therapeutic opportunities, *Blood Journal*, blood-2024025319. https://doi.org/10.1182/blood.2024025319

[16] Dhawan S. S., Avati Nanjundappa, R. P., Branch, J. R., Taylor, W. R., Quyyumi, A. A., Jo, H., McDaniel, M. C., Suo, J., Giddens, D., & Samady, H. (2010) shear stress and plaque development, *Expert Review of Cardiovascular Therapy*, *8(4)*, 545–556. https://doi.org/10.1586/erc.10.28

[17] Krejza, Jaroslaw, Michal Arkuszewski, Scott E. Kasner, John Weigele, Andrzej Ustymowicz, Robert W. Hurst, Brett L. Cucchiara & Steven R. Messe (2006) Carotid artery diameter in men and women and the relation to body and neck size, *Stroke, 37(4),* 1103-1105. https://doi.org/10.1161/01.STR.0000206440.48756.f7

[18] Conti Michele, Chris Long, Michele Marconi, Raffaella Berchiolli, Yuri Bazilevs & Alessandro Reali. "Carotid artery hemodynamics before and after stenting: A patient specific CFD study, *Computers & Fluids 141* 62-74. https://doi.org/10.1016/j.compfluid.2016.04.006

[19] Ngo Dac Hong An, Seung Bae Hwang & Hyo Sung Kwak (2025) Impact of carotid artery geometry and clinical risk factors on carotid atherosclerotic plaque prevalence, *Journal of Personalized Medicine* 15(4), 152, https://doi.org/10.3390/jpm15040152

[20] Modi K, Soos MP & Mahajan K. Stent Thrombosis (2023, July 2025]. Treasure island (FL). *StatPearls Publishing*. https://www.ncbi.nlm.nih.gov/books/NBK441908/

[21] Strecker, Christoph, Axel Joachim Krafft, Lilli Kaufhold, Markus Hüllebrandt, Susanne Weber, Ute Ludwig, Martin Wolkewitz, Anja Hennemuth, Jürgen Hennig, & Andreas Harloff (2020) Carotid geometry is an independent predictor of wall thickness–a 3D cardiovascular magnetic resonance study in patients with high cardiovascular risk, *Journal of Cardiovascular Magnetic Resonance 22*,1-12. https://doi.org/10.1186/s12968-020-00657-5

[22] Stevens, Joseph Robert, Ava Zamani, James Ian Atkins Osborne, Reza Zamani & Mohammad Akrami (2021) Critical evaluation of stents in coronary angioplasty: A systematic review, *Biomedical Engineering Online*, *20(1)*, 46. https://doi.org/10.1186/s12938-021-00883-7

[23] Lichota, Anna, Eligia M. Szewczyk & Krzysztof Gwozdzinski (2020) Factors affecting the formation and treatment of thrombosis by natural and synthetic compounds, *International Journal of Molecular Sciences*, *21(21)*, 7975. https://doi.org/10.3390/ijms21217975

[24] Shaw, Joseph R., Stephan Nopp, Benedicte Stavik, Kimberley Youkhana, Alison L. Michels, Soetkin Kennes, Janusz Rak & Hugo Ten Cate (2025) Thrombosis, translational medicine, and biomarker research: Moving the needle, *Journal of the American Heart Association*, 14(1), e038782. https://doi.org/10.1161/JAHA.124.038782

[25] Noor, A. Fahmi Huwaidi M., Nasrul Hadi Johari, Adi Azriff Basri & Xiao Yun Xu. (2024) Comparison of velocity profiles in stented carotid artery bifurcation between computational fluid dynamics and particle image velocimetry measurements. *International Journal of Automotive and Mechanical Engineering*, *21(2)*, 11386-11397, https://doi.org/10.15282/ijame.21.2.2024.16.0879

[26] Zabidy, Muhamad Luqman Mohd, Muhammad Rafiuddin Ekhwan, and Muhammad Syamil. (2025) "Modeling of the External Airflow in Mountain with Different Velocity and Turbulence Models." Semarak Journal of Thermal Fluid Engineering 5.1: 36-45. https://doi.org/10.37934/sjotfe.5.1.3645a

[27] Sousa, Luisa Costa, Catarina F. Castro & Carlos Conceição António. (2012) Blood flow simulation and applications. In: Natal Jorge R., Tavares J., Pinotti Barbosa M., Slade A. (eds), *Technologies for Medical Sciences, Lecture Notes in Computational Vision and Biomechanics*, (pp. 67-86). Springer, Dordrecht. https://doi.org/10.1007/978-94-007-4068-6_4

[28] Asral, Muhammad, Ridwan Abdurrahman, Nurnabila Syuhada Azian, Ishkrizat Taib, Wu Shunfann, Yap Wee Hang, Yeap Swee Hong, Melchiades Joeffrey Jr, Feblil Huda, and Awaludin Martin. (2024) "CFD Analysis on Double Leaks of Subsea Pipeline Leakage." *Journal of Advances in Fluid, Heat, and Materials Engineering* 1, no. 1: 10-26. https://doi.org/10.37934/afhme.1.1.1026a

[29] Khairi @ Rosli, Nur Afikah, Mohd Azrul Hisham Mohd Adib, Nur Hazreen Mohd Hasni & Mohd Shafie Abdullah (2021) Effect of hemodynamic parameters on physiological blood flow through cardiovascular disease (CVD) – The Perspective Review, *Journal of Advanced Research in Fluid Mechanics and Thermal Sciences*, *74(1)*, 19-34, https://doi.org/10.37934/arfmts.74.1.1934

[30] Azam, Syafiqah Ruqaiyah Saiful, Shaiful Fadzil Zainal Abidin, Izuan Amin Ishak, Amir Khalid, Norrizal Mustaffa, Ishkrizat Taib, Safra Liyana Sukiman, and Nofrizalidris Darlis. (2023) "Flow analysis of intake manifold using computational fluid dynamics." *International Journal of Integrated Engineering* 15, no. 1: 88-95. https://doi.org/10.30880/ijie.2023.15.01.008

[31] Kumar, Bholu, Vivek Kumar Srivastav, Anuj Jain, and Akshoy Ranjan Paul. "Study of numerical schemes for the CFD simulation of human airways." *International Journal of Integrated Engineering* 11, no. 8 (2019): 32-40. https://doi.org/10.30880/ijie.2019.11.08.005

[32] Akram M. Shaaban & André J. Duerinckx (2000) Wall shear stress and early atherosclerosis: A review, *American Journal of Roentgenology*, 174(6), 1487-1542, https://doi.org/10.2214/ajr.174.6.1741657

[33] Abhilash Hebbandi Ningappa, Suraj Patil, Gowrava Shenoy Belur, Augustine Benjamin Valerian Barboza, Nitesh Kumar, Raghuvir Pai Ballambat, Adi Azriff Basri, Shah Mohammed Abdul Khader & Masaaki Tamagawa (2022) Influence of altered pressures on flow dynamics in carotid bifurcation system using numerical methods, *Journal of Advanced Research in Fluid Mechanics and Thermal Sciences*, *97(1)*, 47-61, https://doi.org/10.37934/arfmts.97.1.4761

[34] Dolan, Jennifer M., John Kolega & Hui Meng. (2013) High wall shear stress and spatial gradients in vascular pathology: A review, *Annals of Biomedical Engineering*, *41(7)*, 1411–1427. https://doi.org/10.1007/s10439-012-0695-0

[35] Mahbubi, M. (2025). Comparative Study of Internal Flow Dynamics Using CFD: T-Junction Pipe Geometry. *Semarak Journal of Thermal Fluid Engineering*, *5*(1), 11-20. https://doi.org/10.37934/sjotfe.5.1.1120a

[36] Mat, Annur Adilia Maisarah. (2025) "A Comparative Study of Internal Flow Dynamic Using CFD: Simulation of Turbulent Flow in Diffuser Pipes." *Journal of Advances in Fluid, Heat, and Materials Engineering* 5.1: 10-18. https://doi.org/10.37934/afhme.5.1.1018a

[37] Acharya, Gayathri, Chi H. Lee & Yugyung Lee. (2012) Optimization of cardiovascular stent against restenosis: Factorial design-based statistical analysis of polymer coating conditions. *PLOS ONE*, *7(8)*, e43100. https://doi.org/10.1371/journal.pone.0043100

[38] Ng, Chee Khoon, Peng How Chai, Sim Nee Ting & Hoo Tien Nicholas Kuan. (2024). The Effect of Compressive Stress on Ultrasonic Pulse Velocity in Concrete for Compressive Strength Prediction. *International Journal of Integrated Engineering*, *16*(4), 222-230. https://doi.org/10.30880/ijie.2024.16.04.026

[39] Paisal, M. S. A., Taib, I., & Ismail, A. E. (2017). Computational Analysis on Stent Geometries in Carotid Artery: A review. *IOP Conference Series Materials Science and Engineering*, *165*, 012003. https://doi.org/10.1088/1757-899x/165/1/012003

[40] Marzuki, Najwa Syafiqa, Anas Abdul Rahman, Ayu Abdul-Rahman, Azzim Rosli, Mohamad Syahfiq Misran, Wan Muhammad Fadhli Arif Wan Zulkafli, and Ramadhan Ahmed Ramadhan Basiddiq. (2022) "Numerical Analysis of Wake Interaction of Darrieus Tidal Turbine in Shallow Water Application." *Journal of Advanced Mechanical Engineering Applications* 3, no. 2: 89-104. https://doi.org/10.30880/jamea.2022.03.02.011